南京航空航天大学

论文集

（二〇一〇年） 第41册

高新技术研究院

南京航空航天大学科技部编

二〇一一年五月

高新技术研究院

高新技术研究院2010年发表论文清单

序号	姓名	职称	单位	论文题目	刊物、会议名称	年、卷、期	类别
1	马骏 郭万林	博士 教授	高新院 高新院	Ultrasound-assisted microwave preparation of Ag-doped CdS nanoparticles	Ultrasonics Sonochemistry	2010年17卷3期	
2	沈荣 郭万林 钟文宇	博士 教授 副教授	高新院 高新院	Hydration valve controlled non-selective conduction of Na+ and K+ in the NaK channel	Biochimica et Biophysica Acta	2010年1798卷8期	
3	左广超 沈荣 马少杰 郭万林	博士 博士 博士 教授	高新院	Transport Properties of Single-File Water Molecules inside a Carbon Nanotube Biomimicking Water Channel	ACS Nano	2010年4卷1期	
4	陆鹏 张助华 郭万林	博士 教授 教授	高新院	Magnetism in armchair BC2N nanoribbons	Appl. Phys. Lett	2010年96卷13期	
5	于培师 佘崇民 郭万林	博士 副教授 教授	高新院	Equivalent thickness conception for corner cracks	International journal of solids and structures	2010年47卷16期	
6	唐纯 沈荣 郭万林 陈长风	博士 博士 教授 教授	高新院	Bending manipulation induced sp2–sp3 bond transition in carbon nanotubes	Journal of Applied Physics	2010年卷108期	
7	寇良志 李春 张子越 陈长风 郭万林	博士 副教授 博士生 教授 教授	高新院 西交大 高新院 美国 高新院	Charge carrier separation induced by intrinsic surface strain in pristine ZnO nanowires	Appl. Phys. Lett	2010年卷97期	
8	吴文志 张助华 陆鹏 郭万林	博士 讲师 博士生 教授	高新院	Electronic and magnetic properties of zigzag graphene nanoribbons with periodic protruded edges	Phys.Rev.B	2010年82卷8期	
9	张助华 陈长风 曾晓成 郭万林	博士 教授 教授 教授	高新院 美国 外校 高新院	Tuning the magnetic and electronic properties of bilayer graphene nanoribbons on Si(001) by bias voltage	Phys.Rev.B	2010年81卷15期	

序号	姓名	职称	单位	论文题目	刊物、会议名称	年、卷、期	类别
10	张助华 曾晓成 郭万林	博士 教授 教授	高新院 外校 高新院	Homogeneous nanocables from double-walled boron-nitride nanotubes using first-principles calculations	Phys.Rev.B	2010 年 82 卷 3 期	
11	张助华 武晓君 郭万林 曾晓成	博士 教授 教授 教授	高新院 外校 高新院 外校	Carrier-Tunable Magnetic Ordering in Vanadium–Naphthalene Sandwich Nanowires	J.AM.CHEM.SOC	2010 年 132 卷 30 期	
12	冠良志 唐纯 郭万林 陈长风	博士 博士 教授 教授	高新院	Tunable Magnetism in Strained Graphene with Topological Line Defect	ACS Nano	2010 年 5 卷 2 期	
13	仇虎 沈荣 郭万林	博士 博士 教授	高新院	Vibrating Carbon Nanotubes as Water Pumps	Nano Res	2010	
14	冠良志 李春 张助华 郭万林	博士 副教授 讲师 教授	高新院 外校 高新院 高新院	Tuning Magnetism in Zigzag ZnO Nanoribbons by Transverse Electric Fields	ACS Nano	2010 年 4 卷 4 期	
15	刘心声 郭万林	教授 教授	高新院 高新院	Persistent cooperators in nature	Journal of Theoretical Biology	2010 年 267 卷期	
16	刘心声 吕波 郭万林	教授 硕士 教授	高新院 高新院 高新院	The size distribution of protein families within different types of folds	Biochemical and Biophysical Research Communications	2011 年 406 卷期	
17	尚婷婷 刘心声	硕士 教授	高新院 高新院	Evolutionary Stability of Indirect Reciprocity in Three-Person Game with Two-Way Implementation Errors	Proceedings of the 7th Conference on Biological Dynamic System and Stability of Differential Equation	2010	
18	李夏飞 刘心声	硕士 教授	高新院 高新院	Conditional Fixation Time of Wright-Fisher Process under Weak Selection	The Proceedings of 2010 International Conference on Probability and Statistics of the International Institute for General Systems Studies	2010	
19	刘红胜 刘心声	硕士 教授	高新院 高新院	活跃连接下 Wright-Fisher 过程的演化动态	生物数学学报	2010 年 25 卷 3 期	
20	阮志伟 刘心声	硕士 教授	高新院 高新院	基于相似性机制的合作策略的随机进化	系统管理学报	2010 年 19 卷 6 期	
21	周兴才	副高	外校	Moment consistency of	Metrika	2010 年 72 卷	

序号	姓名	职称	单位	论文题目	刊物、会议名称	年、卷、期	类别
	刘心声 胡舒合	教授 教授	高新院 高新院	estimators in partially linear models under NA samples		期	
22	郭宇锋 蒋莱 郭万林	教授 博士 教授	高新院	Opening carbon nanotubes into zigzag graphene nanoribbons by energy-optimum oxidation	Phys. Rev. B	2010 年卷 82 期	
23	郭宇锋 张助华 郭万林	教授 博士后 教授	高新院	Selective Oxidation of Carbon Nanotubes into Zigzag Graphene Nanoribbons	J. Phys. Chem. C	2010 年卷 114 期	
24	郭宇锋 郭万林	教授 教授	高新院	Semiconducting to Half-Metallic to Metallic Transition on Spin-Resolved Zigzag Bilayer Graphene Nanoribbons	J. Phys. Chem. C	2010 年卷 114 期	
25	台国安 周建新 郭万林	中级 副高 正高	高新院	Inorganic Salt-Induced Phase Control and Optical Characterization of Cadmium Sulfide Nanoparticles	Nanotechnology	2011 年 21 卷 17 期	
26	张助华 郭万林 曾晓成	中级 教授 教授	高新院 高新院 外校	Tunable magnetism on Si(111)-(2×1) via chemisorption of graphene nanoribbons	Phys. Rev. B	2010 年 82 卷 23 期	
27	郭东杰	副高	高新院	A highly porous Nafion membrane templated from polyoxometalates-based supramolecule composite for ion-exchange polymer-metal composite actuator	Journal of Materials Chemistry	2010,20,10159-10168	
28	郭东杰	副高	高新院	GaN Nanowire Functionalized with Atomic Layer Deposition Techniques for Enhanced Immobilization of Biomolecules	Langmuir	2010,26(23),18382–18391	
29	王文波 戴振东	中级 教授	高新院 高新院	动物机器人的研究现状与发展	机械制造与自动化	2010 年 39 卷 2 期	

序号	姓名	职称	单位	论文题目	刊物、会议名称	年、卷、期	类别
30	李宏凯 戴振东	中级 教授	高新院 高新院	A Semiautonomous Sprawl Robot based on Remote Wireless Control	2010 年 IEEE International Conference on Robotics and Biomimetics 会议上交流	2010	
31	阮鹏 俞志伟 张昊 张晓峰 戴振东	硕士 讲师 讲师 硕士 教授	高新院 高新院 高新院 高新院 高新院	基于 ADAMS 的仿壁虎机器人步态规划及仿真	机器人	2010 年 32 卷 4 期	
32	吴强 吉爱红	硕士 副教授	高新院 高新院	一种测力传感器固有频率的提高与测试术	传感技术学报	2010 年 23 卷 2 期	
33	何青松 张　昊 于　敏 郭东杰 戴振东	博士 讲师 副教授 副研 教授	高新院 高新院 高新院	氧化硅掺杂的全氟磺酸聚合物膜在 IPMC 中的应用	中国科技论文在线	2010 年 5 卷 4 期	
34	樊明明 李宏凯 弓娟琴 瞿志俊 戴振东	硕士 博士 教授	高新院	性别和解剖部位对人体皮肤的摩擦性能的影响	摩擦学学报	2010 年 30 卷 3 期	
35	戴振东 杨志贤	教授 博士	高新院	Macro-/Micro-Structures of Elytra, Mechanical Properties of the Biomaterial and the Coupling Strength between Elytra in Beetles	Journal of Bionic Engineering	2010 年 7 卷 1 期	
36	刑　强 戴振东 王周义	博士 教授 博士	高新院	壁虎运动反力和运动行为的动态同步表示方法	现代电子技术	2010 年 33 卷 1 期	
37	杨志贤 戴振东 郭　策	博士 教授 教授	高新院	Morphology and Mechanical Properties of Cybister Elytra	Chinese Science Bulletin	2010 年 55 卷 8 期	
38	王周义 顾文华 吴　强 吉爱红 戴振东	博　士 硕　士 硕　士 副教授 教　授	高新院	Morphology and reaction force of toe of geckos freely moving on ceiling and walls	Science in China E	2010 年 53 卷 6 期	
39	王周义 王金童	博士 硕　士	高新院	Locomotion behavior and dynamics of geckos freely	Chinese Science Bulletin	2010 年 55 卷 29 期	

序号	姓名	职称	单位	论文题目	刊物、会议名称	年、卷、期	类别
	吉爱红 戴振东	副教授 教　授		moving on the ceiling			
40	何青松 于　敏 丁海涛 郭东杰 戴振东	博士 副教授 硕　士 副　研 教　授	高新院	Effects of Anisotropic Surface Texture on the Performance of Ionic Polymer-Metal Composite (IPMC)	在 2010 年 SPIE -Electroactive Polymer Actuators and Devices (EAPAD) 会议上交流	2010	
41	丁海涛 于　敏 郭东杰 何青松 戴振东	硕士 副教授 副研 博士 教授	高新院	离子聚合物金属复合材料电学性能研究	机械制造	2010 年 26 卷 2 期	
42	张昊 郭东杰 戴振东	中级 副研 教授	高新院	仿壁虎微纳米刚毛阵列的研究进展	科学通报	2010 年 55 卷 6 期	
43	张昊 郭东杰 戴振东	中级 副研 教授	高新院	Progress on gecko-inspired micro/nano-adhesion arrays	Chinese Science Bulletin	2010 年 55 卷 18 期	
44	宋文伟 郭策 马岩 张晓玉 戴振东	硕士 教授 工程师 高工 教授	高新院	仿甲虫鞘翅轻质结构的力学性能研究	机械科学与技术	2010 年 29 卷 10 期	
45	于海武 王晓雷 周飞	正高 教授 教授	机电 051 高新院	Geometric shape effects of surface texture on the generation of hydrodynamic pressure between conformal contacting surfaces	Tribology Letters	2010 年 37 卷 1 期	
46	周飞 岳宾 王晓雷 吴雪梅 诸葛兰剑	教授 教授 教授 教授	高新院 051 051 苏大 苏大	Surface roughness, mechanical properties and bonding structure of silicon carbon nitride films grown by dual ion beam sputtering	*Journal of Alloys and Compounds*	2010 年 492 卷期	
47	周飞 王霄 王美玲 廖文和 陈卫东	正高 高工 教授 教授	高新院 051 06 高新院 高新院	钛合金表面红外隐身涂层的原位制备及性能研究	隐身技术	2010 年 2 期	

序号	姓名	职称	单位	论文题目	刊物、会议名称	年、卷、期	类别
48	周飞 孔志强 廖文和 陈卫东 张靖周	教授 教授 教授 教授	高新院06 高新院 高新院02	稀土Er3+掺杂ZAO薄膜红外发射率研究	隐身技术	2010年2期	
49	王远 周飞 张庆文	中级 教授	西南林大 高新院 西南林大	Al2O3/CrNx复合膜的摩擦磨损特性	材料工程	2010年2期	
50	周飞 吴志威 王美玲 陈康敏	教授 高工 副教授	高新院 高新院06 江大	Structure and mechanical properties of pincers for lobster (Procambarus clarkii) and crab (Eriocheir Sinensis)	*Journal of the Mechanical Behavior of Biomedical Materials*	2010年3卷6期	
51	周飞 岳宾 王谦之 王晓雷 足立幸志 加藤康司	教授 教授 副教授 教授	高新院 高新院051 051 日本东北大学 日本大学	Tribological properties of a-CNx coatings sliding against SiC balls in ethylene glycol aqueous solution	*Lubrication Science*	2010年22卷6/7期	
52	黄小华 涂江平 周飞	中级 教授 教授	高新院 浙大 高新院	Hollow microspheres of NiO as anode materials for lithium-ion batteries	*Electrochimica Acta*	2010年55卷6/7期	
53	洪波 吴雪梅 诸葛兰剑 吴兆丰 周飞	中级 教授 教授 教授	苏大 苏大 苏大 苏大 高新院	Influence of N2 proportion on mechanical properties of SiCN thin films prepared by DIBSD	Advanced Materials Research	2010年97-101卷期	
54	周飞 加藤康司	中级 教授	高新院 日本大学	Friction and wear properties of amorphous carbon nitride coatings in water lubrication：a review	在2010年 The 5th International Conference on Technological Advances of Thin Films & Surface Coatings	2010年	
55	王谦之 周飞 陈康敏	博士 教授 副教授	高新院 高新院 江学	Friction and wear properties of TiCN coatings sliding against	在2010年 The 5th International Conference on	2010年	

序号	姓名	职称	单位	论文题目	刊物、会议名称	年、卷、期	类别
	王美玲 钱涛	高工	06 星湖公司	SiC and steel balls in air and water	Technological Advances of Thin Films & Surface Coatings		
56	黄小华 周飞 孔志强	中级 教授	高新院 高新院	Enhanced violet photoluminescence from Er-doped ZnO:Al thin films prepared by RF magnetron sputtering	在 2010 年 The 5th International Conference on Technological Advances of Thin Films & Surface Coatings	2010 年	
57	李艳霞 王谦之 苏恒 王美玲 陈康敏 周飞	051 051 051 06 苏大 高新院	051 051 051 06 苏大 高新院	Friction and wear properties of CrN coatings sliding against SiC balls in deionized water	在 2010 年 The Second Asian Conference on Mechanics of Functional Materials and Structures (ACMFMS 2010)	2010 年	
58	王政 黄小华 王美玲 周飞	硕士 讲师 高工 教授	06 高新院 06 高新院	Photoluminescence and electronic properties of Al and Er co-doped ZnO thin films prepared by sol–gel method	在 2010 年 The Second Asian Conference on Mechanics of Functional Materials and Structures (ACMFMS 2010)	2010 年	
59	彭玉钧 周飞 王宪良 陈建宁 钱涛 云乃彰	硕士 教授 高技工 教授	05 高新院 051 052 公司 052	微结构与 DLC 薄膜耦合钛合金表面水润滑摩擦学特性研究	在 2010 年全国青年摩擦学学术会议 会议上交流	2010 年	
60	彭玉钧 周飞 王晓楠 孙见君	硕士 教授 教授	05 高新院 051 南林	微坑型表面织构对钛合金水润滑摩擦学性能的影响	在 2010 年第五届全国生物摩擦学与内植物工程学术研讨会 会议上交流	2010 年	
61	于敏 莫桂东 贾世星 郭东杰 戴振东	副高 硕士生 工程师 副教授 教授	高新院 5 院 55 所 高新院 高新院	仿壁虎刚毛阵列的几何结构分析及制备	南京航空航天大学学报	2010 年 42 卷 6 期	
62	丁海涛 于敏 郭东杰 何青松	硕士 副教授 副教授 硕士生	05 高新院 高新院 5 院	离子聚合物金属复合材料电学性能研究	机械制造	2010 年 48 卷 6 期	

序号	姓名	职称	单位	论文题目	刊物、会议名称	年、卷、期	类别
	戴振东	教授	高新院				
63	刘海颖 王惠南 冯成涛	副高 正高 博士	高新院	Attitude Control of Micro-satellite Using Thruster Plus Bias Momentum Wheel	ICIC Express Letters	2010 年 4 卷 4 期	
64	刘海颖 郑罡 王惠南 冯成涛	副高 中级 正高 博士	高新院 071	Research on Integrity Monitoring For Integrated GNSS/SINS System	在 2010 年 The 2010 IEEE International Conference on Information and Automation 会议上交流	2010	
65	刘海颖 叶伟松 王惠南	副高 中级 正高	高新院 高新院	基于 ERAIM 的惯性辅助卫星导航系统完好性检测	中国惯性技术学报	2010 年第 18 卷第 6 期	
66	刘海颖 叶伟松 冯成涛	副高 中级 博士	高新院 高新院	基于 OFDM 信号的无线电定位系统研究	无线电工程	2010 年 40 卷 3 期	
67	刘海颖 杨宇晓 丁尚文 冯成涛	副高 中级 博士 博士	高新院 高新院 031 031	地面站频率不稳定对航天器跟踪性能影响的分析	系统工程与电子技术	2010 年 32 卷 4 期	
68	周小明 黄护林	博士 教授	02 高新院	MHD effects on the instability of thermocapillary convection in two-layer fluid system	International Journal of Heat and Mass Transfer	2010 年 53 卷 25-26 期	
69	周小明 黄护林	博士 教授	02 高新院	MHD effects on the critical temperature differences of oscillatory thermocapillary convection in two-layer fluid system	Frontiers of Energy and Power Engineering in China	2010 年 4 卷 2 期	
70	周小明 黄护林	博士 教授	02 高新院	MHD Effect on Interfacial Deformation of Thermocapillary Convection in Two-Layer System	Microgravity Science Technology	2010 年 22 卷 2 期	
71	周小明 黄护林	博士 教授	02 高新院	Numerical Simulation of Steady Thermocapillary Convection in a Two-Layer System Using Level Set Method	Microgravity Science Technology	2010 年 22 卷 2 期	

序号	姓名	职称	单位	论文题目	刊物、会议名称	年、卷、期	类别
72	周小明 黄护林 蔡亮	博士 教授 博士	02 高新院 02	基于 Leverl Set 方法的双层流体热毛细对流的数值研究	工程热物理学报	2010 年 31 卷 3 期	
73	周小明 黄护林	博士 教授	02 高新院	大尺度环形液池内双层流体热毛细对流不稳定性	在 2010 年 中国工程热物理学会 会议上交流	2010	
74	蔡亮 黄护林	博士 教授	02 高新院	轴向磁场作用下圆柱绕流的三维流动特性研究	在 2010 年 中国工程热物理学会 会议上交流	2010	
75	王磊磊 黄护林	博士 教授	02 高新院	低温超导馈线系统的有限元热分析	在 2010 年 Power and Energy Engineering Conference 会议上交流	2010	
76	高益兵 黄护林	硕士 教授	02 高新院	A Parametric Study of Characteristics of Concentrating PV modules	International Journal of Low-Carbon Technologies	2010 年 5 卷 2 期	
77	李博 黄护林	硕士 教授	02 高新院	Heat transfer enhancement of free surface MHD-flow by a protrusion wall	Fusion Engineering and Design	2010 年 85 卷 7-9 期	
78	李江烨 黄护林	硕士 教授	02 高新院	Effect Of Magnetic Field On Blood Flow And Heat Transfer Through A Stenosed Artery	在 2010 3rd International Conference on Biomedical Engineering and Informatics 会议上交流	2010	
79	吴小翠 黄护林	硕士 教授	02 高新院	几何参数对高温吸收器热性能的影响	在 2010 年 中国工程热物理学会 会议上交流	2010	
80	吴小翠 黄护林	硕士 教授	02 高新院	Numerical simulation of a high temperature solar thermal receiver	在 2010 9th International Conference on Sustainable Energy Technologies 会议上交流	2010	
81	周慧 黄护林	硕士 教授	02 高新院	不同基底材料对珠状凝结换热的影响	在 2010 中国工程热物理学会 会议上交流	2010	
82	曲小雷 曹云峰	硕士 教授	03 高新院	基于 ARM 的空中机器人飞行控制系统的设计	工矿自动化	2010 年 36 卷 1 期	

序号	姓名	职称	单位	论文题目	刊物、会议名称	年、卷、期	类别
83	庄丽葵 丁萌 曹云峰	中级 博士 教授	高新院 03 高新院	利用地平线与跑道边缘估计无人机着陆参数	传感器与微系统	2010 年 29 卷 3 期	
84	庄丽葵 王彪 谢娟 曹云峰	中级 副高 硕士 教授	高新院 031 03 高新院	基于 DODAF 的无人机 FMCS 体系结构设计	价值工程	2010 年 29 卷 7 期	
85	赵滨 庄丽葵 王彪 曹云峰	硕士 中级 副高 教授	03 高新院 031 高新院	微型飞行器动力学模型的系统辨识	科学技术与工程	2010 年 33 卷 10 期	
86	胡剑华 庄丽葵 王彪 曹云峰	硕士 中级 副高 教授	03 高新院 031 高新院	基于 S3C2440 的嵌入式自动驾驶仪硬件设计与实现	科学技术与工程	2010 年 10 卷 34 期	
87	刘兴华 曹云峰	博士 教授	03 高新院	Design of UAV Fight Control System Virtual Prototype using Rhapsody and Simulink	在 2010 年 6 月 25-27 日举行的国际会议上交流	2010 年 1 卷 3 期	
88	邹小志 曹云峰	硕士 教授	03 高新院	一种改进的微型飞行器非线性动态逆解耦控制研究	航空兵器	2010 年 卷 4 期	

Ultrasonics Sonochemistry 17 (2010) 534–540

Contents lists available at ScienceDirect

Ultrasonics Sonochemistry

journal homepage: www.elsevier.com/locate/ultsonch

Ultrasound-assisted microwave preparation of Ag-doped CdS nanoparticles

Jun Ma, Guo'an Tai, Wanlin Guo *

Institute of Nanoscience, Nanjing University of Aeronautics and Astronautics, No. 29, Yudao Street, Nanjing 210016, PR China

ARTICLE INFO

Article history:
Received 28 September 2009
Received in revised form 9 November 2009
Accepted 13 November 2009
Available online 18 November 2009

Keywords:
Ultrasound
Microwave
Ag–CdS
Phase evolution
Raman enhanced
Photocatalysis

ABSTRACT

Ag-doped CdS nanoparticles were synthesized by an ultrasound-assisted microwave synthesis method. The X-ray diffraction patterns reveal a structural evolution from cubic to hexagonal with increasing molar ratios of Ag^+/Cd^{2+} from 0% to 5%. It shows that the Ag-doped hexagonal CdS nanoparticles are polycrystal. The X-ray photoelectron spectroscopy of the CdS nanoparticles doping with 5% Ag^+ shows that the doped Ag in CdS is metallic. Simultaneously, the characteristic Raman peaks of the CdS nanoparticles enhance with increasing Ag^+ concentrations. The photocatalytic activity of different Ag-doped samples show a reasonable change due to different ratios of Ag which doped into CdS.

1. Introduction

Doping is important for semiconductors, which plays a critical role in tunning their optical and electrical properties [1] for the potential applications in wavelength-controlled lasers [2], biotechnology [3], and solar cells [4]. In particular, photoluminescence emission and excitation wavelength of nanocrystals may be tuned by dopants [5]. The lasing threshold of semiconductor nanocrystals can be reduced three fold by adding extra electrons [6]. In addition, in the bioimage field, less harmful dopants can mitigate the toxic problem by producing visible or infrared emission instead of harmful elements currently used [7]. Meanwhile, doping the semiconductors with noble metals as the photoinduced electron acceptors can also enhance the ability of photocatalysis [8]. Also, some experiments have conformed that by means of small amounts of metal doping, the crystallization progress of semiconductors can be affected [9].

CdS is one of the most important II–VI semiconductors with a direct bulk phase band gap of 2.4 eV at room temperature, It is extensively used for optoelectronic devices because of its tuning emission in the visible-light range with different sizes and shapes. CdS has the great potential applications as nanoelectronics and photocatalytic materials [10,11]. In recent years, doping of CdS nanostructures has attracted intensive attentions. A new peak appeares in the Mn-doped CdS nanocrystals photoluminescence spectra due to Mn d–d transitions [12]. Se doping can induce the formation of branched CdS nanocrystals and cause the red shift of photoluminescence of CdS nanocrystals [13,14]. (Mn, Zn) co-doped CdS nanowires exhibit a room-temperature ferromagnetic behavior [15]. Particularly, Ag is a group IB element. The potential difference between the Fermi level of Ag and the conduction band of semiconductors facilitates the electron transfer between the semiconductor matrix and the doped metal [16]. Ag doping can provide a convenient way to tailor the physical properties of the intrinsic semiconductor such as Raman scattering [17] and photocatalysis [18]. However, Ag is an active metal which can be easily oxidized by the general doping method. Impurities such as Ag easily diffuse even at room temperature [19]. Therefore, it remains an important challenge to dope Ag into CdS nanocrystals.

Microwave irradiation has been proven to be a useful tool in synthesizing nanomaterials with enhanced reaction rate [20,21], but has some disadvantages such as limited thickness penetrating and poorly experimental repeatability [22]. Simultaneously, sonochemistry method has been widely used to synthesis nanomaterials [23,24]. Tai and Guo have developed a sonochemistry-assisted microwave method for controlled synthesis of semiconductor nanostructural materials [25].

Here, the ultrasound-assisted microwave synthesis method has been successfully used to dope Ag into CdS nanoparticles. It was observed that Ag doping of CdS nanoparticles can induce the evolution of crystal structure from cubic to hexagonal under the synergistic effect of ultrasound and microwave. The characteristic Raman peaks of CdS have been enhanced with increasing Ag^+ concentrations. Photocatalytic activity experiment indicated that the Ag clusters have doped into the CdS matrix.

* Corresponding author. Tel./fax: +86 25 84895827.
E-mail address: wlguo@nuaa.edu.cn (W. Guo).

1350-4177/$ - see front matter © 2009 Elsevier B.V. All rights reserved.
doi:10.1016/j.ultsonch.2009.11.008

2. Experimental section

2.1. Materials

Sulfur powders, cadmium acetate and thioacetamide were purchased from Shanghai Chemical Reagents Company. Silver nitrate was purchased from Shanghai Shenbo Chemical Co. Ltd. Rhodamine B was purchased from Tianjin Institute of Chemical Reagents. All chemicals are analytical grade products and used without further purification.

2.2. Synthesis of Ag-doped CdS Nanoparticles

In typical synthesis process, 2.5 mmol of $Cd(CH_3COO)_2{\cdot}2H_2O$, 1.25 mmol of CS-$(NH_2)_2$ and 1.25 mmol of sulfur powders were dissolved into 50 ml of ethylene glycol (EG). The mixed solution was transferred to a three-necked flask, stirred for 15 min, and then was purged for 5 min with Argon gas before put into the microwave reactor. The resulting mixed solution was placed in a program-controlled ultrasound-assisted microwave reactor (see Ref. [25]) with the microwave power set at 400 W and operated at 140 °C for 15 min. In this process, a high-intensity ultrasonic probe (from Xinzhi Co., China, JY92–2D, with a 10 mm diameter titanium horn of 20 kHz and 400 W working in a pulsed mode with a duty cycle of 0.5 s) was directly immersed in the solution. The Ti horn was immersed into the solution for 1 cm. In addition, a condenser was attached to the three-necked flask. After the reaction, the resulting solution was poured into cool cyclohexylamine and preserved at 5 °C for 12 h. To obtain Ag-doped products with different concentrations, the above reaction process was repeated by just adding 0.025 mmol (1% Ag^+), 0.075 mmol (3% Ag^+) and 0.125 mmol (5% Ag^+) of $AgNO_3$ into the initial reaction mixtures respectively. The as-synthesized products were separated by centrifugation, washed with absolute ethanol and ultrapure water (resistivity 18 MΩ-cm) several times, and dried at 60 °C in vacuum for 12 h.

2.3. Structural characterization

The phase of the as-synthesized products was detected by a Bruker D8 Advance diffractometer which was operating at 40 kV and 40 mA (CuK_α irradiation, $\lambda = 1.542$ Å). TEM, High-resolution TEM (HR-TEM) images and the typical selected area electron diffraction (SAED) patterns were recorded on a JEOL JEM-2100F microscope operating at 200 kV. For this characterization, the products were ultrasonically dispersed in ethanol, then, the resulting suspensions were dropped onto the ultrathin carbon-coated copper grids. X-ray photoelectron spectroscopy (XPS) data were obtained with a Thermo ESCALAB 250 using a 150 W AlK_α radiation. The Resonant Raman spectra were measured on a Renishaw Raman spectrometer system under the excitation of a 514.5 nm line out of a 20 mW Argon Ion laser. Room temperature UV–visible absorption spectra were recorded on a Vary 500 spectrometer.

2.4. Photocatalytic study

The photocatalytic activity of the as-synthesized products for degrading Rhodamine B aqueous solution was studied with a 150 W metal halide lamp ($\lambda > 380$ nm) being used as a visible-light source. First, the suspensions containing the as-synthesized samples (100 mg) and Rhodamine B (4 mg/L, 150 mL) were stirred in the dark for 15 min to obtain an adsorption and desorption equilibrium between the catalyst and Rhodamine B. Then the suspensions were placed under the metal halide lamp. At a designed time intervals, 4 mL of the aqueous solution was taken out for analysis. The photocatalytic activity of the catalyst was evaluated by detecting the visible absorbance characteristic of targeted Rhodamine B using a Vary 500 spectrometer.

3. Results and discussion

3.1. Structure and morphology of the Ag-doped CdS nanoparticles

Fig. 1 displays the XRD patterns of the Ag-doped CdS nanoparticles with different Ag^+/Cd^{2+} molar ratios in the initial reaction system synthesized in the sonochemistry-assisted microwave reactor. The reflection peaks of pure CdS in Fig. 1a can be indexed as zinc-blende structure (space group $F\bar{4}3m$) with the lattice constant of $a = 5.800$ Å, in agreement with literature values (JCPDS Card No. 10-0454). However, the reflection peaks of CdS with 5% Ag^+ dopant in the initial reactants in Fig. 1d correspond to the hexagonal wurtzite phase (space group $P63mc$) with the lattice constants of $a = b = 4.141$ Å and $c = 6.720$ Å (JCPDS Card No. 41-1049). The crystal structure evolution of the samples from the cubic to the hexagonal phase is noticeable from the gradual enhanced hexagonal characteristic peaks such as those at 2θ equal to 28.1° and 51.9° with increasing Ag^+ concentrations. In Fig. 1b and c can be considered as the transition-state between the cubic and the hexagonal phase. No obvious diffraction peaks of any other minerals can be detected in the XRD patterns. There are no obvious characteristic peaks of Ag or Ag_2S can be observed, indicating that the Ag has immersed into the CdS nanoparticles matrixes. In order to get nanocrystalline size-change information, the Scherer formula [26] was used to calculate the average size of the nanocrystallines

$$d = \frac{0.94\lambda}{B\cos\theta}$$

Here, d is the diameter of the crystallite, λ is the wavelength of X-ray radiation, B is the corrected full-width at half-maximum (FMWH) of the peak, and θ is the angle of diffraction. The (1 1 1), (2 2 0) and (3 1 1) crystal planes were used to calculate the average size of the cubic crystallites, while the (0 0 2), (1 1 0) and (1 1 2) crystal planes were used to calculate the average size of the hexagonal crystallites. The calculated results were showed in Table 1.

The TEM images of the Ag-doped CdS (with 5% Ag^+ in the reactants) were exhibited in Fig. 2. It is found that most of the crystallites are spherical and their size of is ~15 nm which agrees with the XRD result (see Table 1). The corresponding selected area electron diffraction pattern (Fig. 2b) was recorded on the nanoparticles. The diffraction ring can be indexed to the (0 0 2), (1 1 0) and (1 1 2) planes, confirming the wurtzite phase. HR-TEM in Fig. 2d

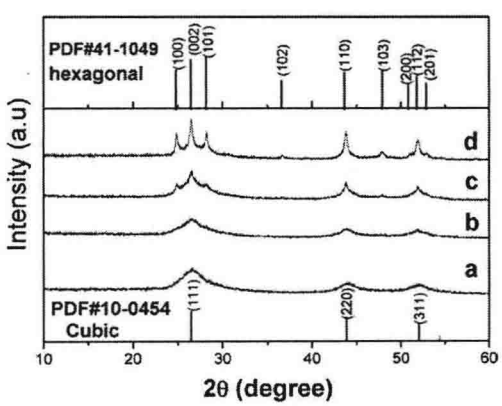

Fig. 1. XRD patterns of the as-synthesized Ag-doped CdS nanoparticles with different Ag^+ molar ratios in the reactants: (a) pure CdS; (b) 1% Ag^+ (0.025 mmol $AgNO_3$); (c) 3% Ag^+ (0.075 mmol $AgNO_3$); and (d) 5% Ag^+ (0.125 mmol $AgNO_3$).

Table 1
The calculated CdS nanocrystallite size from XRD patterns with different molar ratios of Ag^+ in the reactants: (a) pure CdS; (b) 1% Ag^+ (0.025 mmol $AgNO_3$); (c) 3% Ag^+ (0.075 mmol $AgNO_3$); and (d) 5% Ag^+ (0.125 mmol $AgNO_3$).

Sample	XRD size (nm)
a	4.07
b	4.56
c	7.35
d	16.18

also shows the preferred orientation along [0 0 1] which is consistent with the XRD result.

The XPS analysis of Ag-doped CdS (with 5% Ag^+ dopants in the reactants) nanoparticles is given in Fig. 3. From Fig. 3b and c, it is obvious that the binding energy of peaks $Cd3d_{5/2}$ and $S2p_{3/2}$ are 404.47 and 160.92 eV, respectively. The $Ag3d_{5/2}$ peak is centered at 367.45 eV; whereas, the $Ag3d_{3/2}$ is found at 373.53 eV with a spin energy separation of 6.08 eV. This is characteristic of metallic Ag [17]. It is also obtained that the real Ag-doped molar ratio is about 1.43% from XPS which is lower than the Ag^+ concentration in the initial reactants.

3.2. Investigation of the synthesis and phase evolution mechanism

In order to investigate the contributions of ultrasound and microwave, some blank tests have been taken: (1) only microwave; (2) only ultrasound; and (3) mechanical stirring. As a result, the expected products could not be obtained by the above three methods. If prepared by pure microwave, plenty of residual sulfur powders can be found in the resulting products. The reaction should last a much longer time and the products are not ideal when only ultrasound or only mechanical stirring is used. It's indicated that ultrasound-assisted method is a convenient and quick approach to prepare Ag-doped CdS nanoparticles.

The energy of the microwave photon (0.0016 eV) is too low to break chemical bonds and is also lower than the energy of Brownian motion. It is therefore clear that microwaves cannot induce chemical reactions. Microwave-enhanced chemistry is based on the efficient heating of materials by "microwave dielectric heating" effects [27]. On the other hand, there two regions in sonochemical reactivity as postulated by Suslick et al. [28]: the gas phase within the collapsing cavity and the interface between the liquid and bubble. As in this experiment, microwave can be used as a quick and homogeneous heater. Simultaneously, pulsed ultrasound can offer a high energy to dissolve sulfur powder and penetrate Ag into CdS matrix. Therefore, the ultrasound-assisted microwave method can be used to prepare homogeneous doped products.

What is the phase evolution mechanism? The stacking sequence of wurtzite is ABAB and it transforms to ABCABC for zinc-blende. In both of the structures, cadmium and sulfur atoms are tetrahedrally coordinated. In thermodynamics, it is notable that zinc-blende is the most stable form at lower temperature for bulk phase, while wurtzite is more stable at high temperature. However, the situation is different in nanoscale. Banerjee et al. [29] has reported the size-dependent structural phase transformation of CdS nanoparticles. Zinc-blend to wurtzite evolution involves only a change in symmetry. The nucleation and growth of nanocrystals are primarily governed by the competition between the surface and volume free energies. During the nucleation, symmetry favors the cubic crystal structure for spherical nucleus over hexagonal structure by adopting low-energy (1 1 1) facets on the nanocrystal surface. From Table 1, the size of the crystallites grows

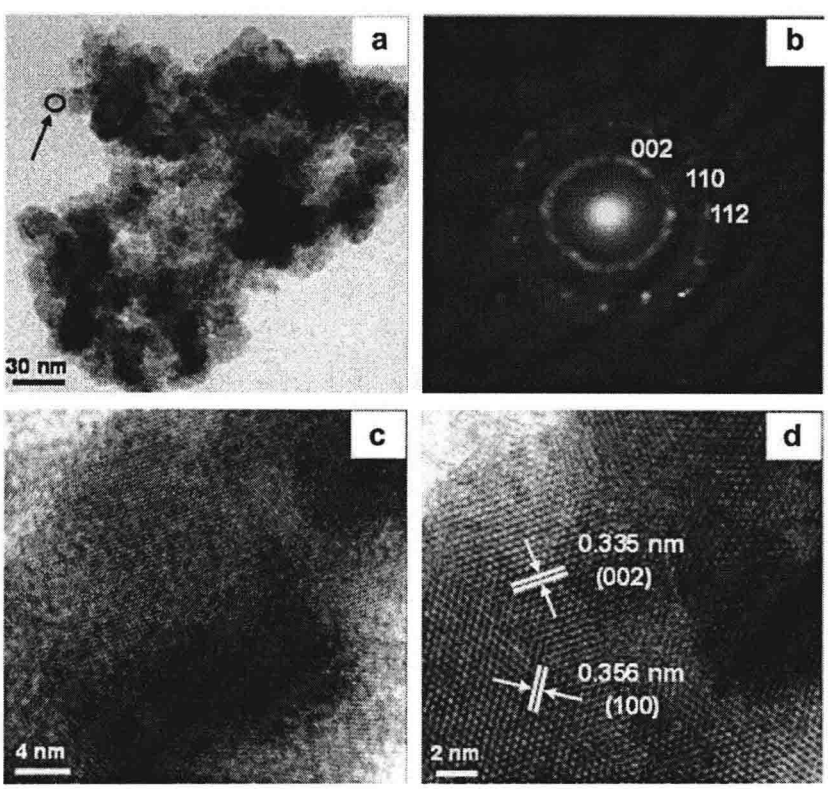

Fig. 2. TEM images of Ag-doped CdS nanoparticles with 5% Ag^+ (0.125 mmol $AgNO_3$) in the reactants: (a) TEM image of the sample; (b) SEAD pattern corresponds to the white ring area in (a); (c and d) high-resolution TEM images of the as-synthesized sample.

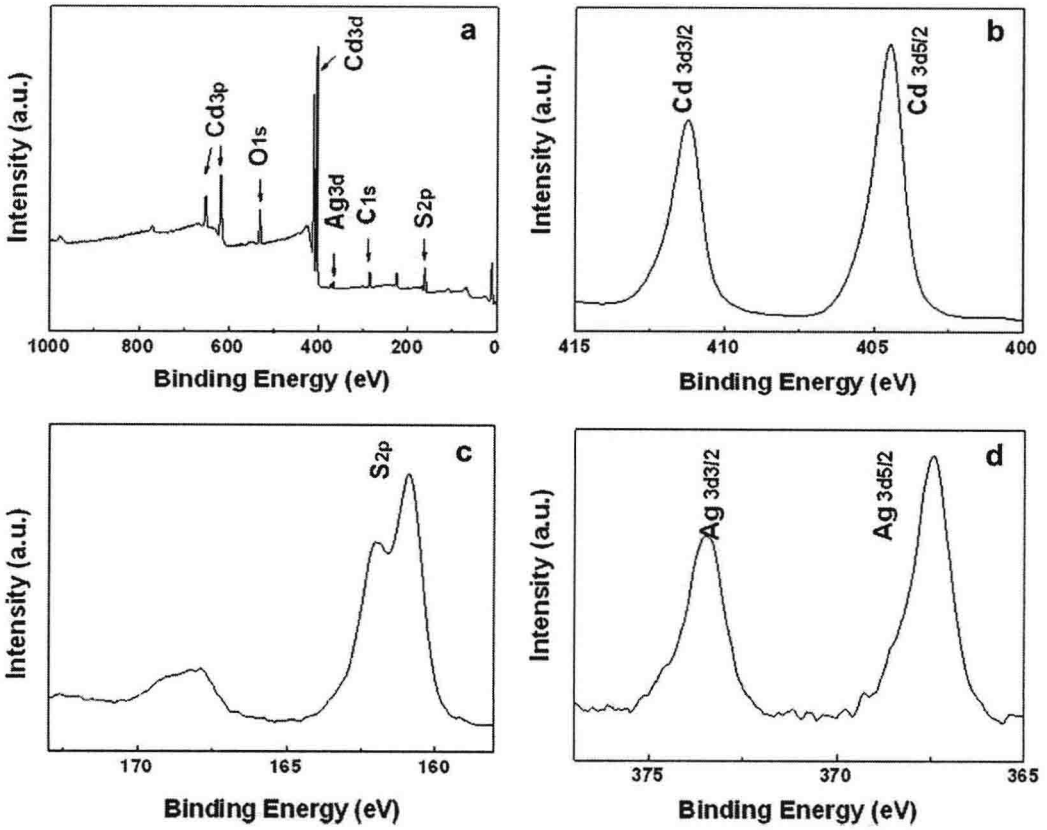

Fig. 3. XPS survey spectrum of the as-synthesized Ag-doped CdS with 5% Ag^+ (0.125 mmol $AgNO_3$) in the reactants. (a) Full spectrum; (b) Cd3d spectrum; (c) S2p spectrum; and (d) Ag3d spectrum.

with increasing the Ag^+ concentrations, therefore, the crystal structure evolves from cubic to hexagonal naturely, and the critical transformation size of CdS nanocrystallites is around 4–7 nm which agrees with Banerjee's report. It is reasonable that the CdS nanocrystallites transform from a cubic structure at the initial stage of nucleation to the stable hexagonal structure as the crystallite size increases, following Ag^+ into the CdS matrixes with the help of ultrasound. Ag^+ ions probably changes the free energy of the system and thus induce the fcc (face centered cubic) to hcp (hexagonal closest packed) phase transformation.

3.3. Raman investigation

To verify the Ag atomic clusters in CdS nanoparticle matrixes, the characteristic Raman spectra of CdS nanoparticles undoped and doped with different Ag concentrations were investigated. It is found that the main peaks at about 301 cm^{-1} and 602 cm^{-1} are obtained in Fig. 4, corresponding to 1LO and 2LO of CdS. The 1LO peak of the as-synthesized samples shows a small degree of asymmetric broadening towards the low frequency side. This can be ascribed to the contribution of the vibrational modes selected by the resonance of the exciting and the scattered light with the confined excitonic states [30]. It's easy to find out that the Ag-doped products show a gradual enhancement with increasing the Ag^+/Cd^{2+} ratios from 1% to 5% in the initial reactants. Surprisingly, the product doping with 5% Ag^+ shows more than 4-fold enhancement at 1LO peak compared with the pure CdS sample. And a weak 3LO peak at around 900 cm^{-1} can be first observed the CdS nanoparticles doping with 5% Ag^+, this peak can be observed more clearly when the Ag^+/Cd^{2+} ratio has increased to 10% (not shown here). Both the theoretical and experimental studies have suggested that the enhanced signals in the characteristic Raman spectra are mainly attributed to electromagnetic excitation of localized surface plasmon of noble metals [31,32]. So, the Raman enhancement is mainly owing to the electrons transferred between CdS and Ag [17]. It's indicated that Ag has penetrated into CdS nanoparticle matrix in the form of atom clusters which agrees with the XPS patterns and the TEM figures. In addition, the background of the Raman spectra of 5% Ag-doped CdS sample should be attributed to the emission of the CdS nanoparticles [33].

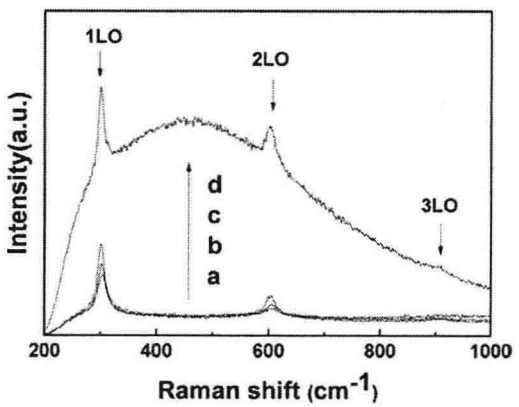

Fig. 4. Raman spectra of the as-synthesized Ag-doped CdS nanoparticles with different Ag^+ molar ratios in the initial reactants, from bottom up: (a) pure CdS; (b) 1% Ag^+ (0.025 mmol $AgNO_3$); (c) 3% Ag^+ (0.075 mmol $AgNO_3$); (d) 5% Ag^+ (0.125 mmol $AgNO_3$).

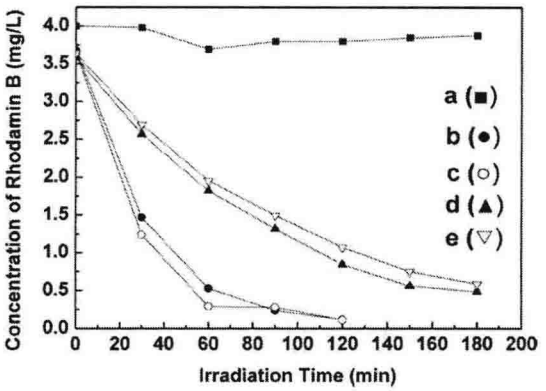

Fig. 5. Photocatalytic degradation activity for Rhodamine B obtained from the as-synthesized Ag-doped CdS nanoparticles with different Ag^+ molar ratios in the reactants: (a) without any presence of catalysts; (b) pure CdS; (c) 1% Ag^+ (0.025 mmol $AgNO_3$); (d) 3% Ag^+ (0.075 mmol $AgNO_3$); and (e) 5% Ag^+ (0.125 mmol $AgNO_3$).

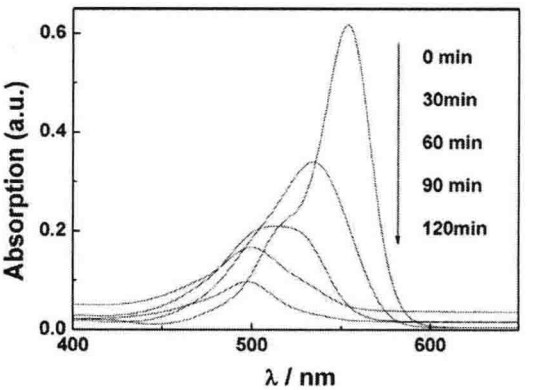

Fig. 6. Absorption spectra changes of Rhodamine B solutin (4 mg/L,150 mL) in the presence of 100 mg Ag-doped CdS nanoparticles (with 1% Ag^+ in the reactants) under visible-light irradiation as time increasing.

3.4. Photocatalytic activity study of Ag-doped CdS

The photocatalytic performance of the different Ag-doped CdS nanoparticles was evaluated by photocatalytic degradation of Rhodamine B aqueous solutions. It is important that the as-synthesized samples showed an obviously photocatalytic activity for Rodamine B degradation under the visible-light irradiation. In order to evaluate the photocatalytic activity of the as-synthesized samples, the photocatalytic experiments for the as-synthesized samples with various Ag^+/Cd^{2+} doping ratios in the same system were carried out respectively. The concentration changes of Rhodamine B solutions versus irradiation time are shown in Fig. 5, and the fitting results of the pseudo-first order kinetics equation are listed in Table 2. No obvious change was found without presence of any catalyst (a), and this can exclude the thermal effect in the experimental progress. The results indicated the half-life time for the degradation of Rhodamine B was 23 min (sample b), 19 min (sample c), 61 min (sample d) and 68 min (sample e), respectively, which obeyed the pseudo-first order kinetics well [34]. Additionally, Fig. 5 points out that Ag-doped CdS nanoparticles (sample c with 1% Ag^+ in the initial reactants) have exhibited nearly the same photocatalytic activity with pure CdS, but better than other doped samples. The reason has been presented as follows.

Fig. 6 shows the variation of the absorption spectra of Rhodamine B in the presence of Ag-doped CdS (with 1% Ag^+ in the reactants) under the visible-light for various irradiation times. It is well known that Rhodamine B is stable without catalyst in visible-light region. However, Rhodamine B solution can be significantly degraded in the presence of as-synthesized CdS nanoparticles. The characteristic sharp peak at 554 nm gradually diminished and the peak shifted to lower wavelength simultaneously with time increasing. Rhodamine B was almost decomposed completely for about 60 min irradiation. It is ascribed the peak shift to N-de-ethylation of Rhodamine B to Rhodamine in the degradation progress, as has been confirmed by Watanabe et al. [35].

It is obviously that the CdS nanoparticles doped with 1% Ag^+ in the initial reactants had a better photocatalytic activity than other doped samples, but nearly the same with pure CdS. The bottom of conduction band and the top of valance band (BCB and TVB) of CdS in aqueous solution is −4.0 and −6.5 eV [36]. From XRD, XPS and Raman results, the existence of metallic Ag in CdS can be ascribed to Ag atomic clusters which could be expressed as Ag_n. And the energy level of Ag atomic cluster changes from −1.3 eV ($n = 1$) to −4.64 eV of bulk phase ($n = \infty$) [37]. As Ag clusters are immersed into CdS nanoparticles, the electrons transformation schematic is displayed in Fig. 7. The photocatalytic activity can not change when the electrons could not transfer from BCB of CdS to Ag_n due to the energy level of Ag_n is much higher than BCB when the Ag doping ratios is small. As the n increasing, the energy level of Ag_n decreases gradually and starts to accept photoinduced electrons effectively from BCB when the Ag_n energy levels lie close to BCB. Photoinduced electrons would directly generate on the Ag_n energy levels when they lie lower than BCB. Simultaneously, the electrons transfer to O_2 which absorbed on CdS. The major role of the Ag atomic clusters is attributed to acceleration of $O_2^{\cdot-}$ formation, with effect of decreasing recombination to increase the activity of catalysis. The sample c shows a slight enhancement and nearly the same activity compared to pure CdS due to the doping ratio is not optimum to enhance the activity a lot. As n increases to a sufficient large number, when the energy level of Ag_n is lower than the energy level of O_2 which absorbed on CdS, the electron can not transfer to O_2, then the Ag_n begins to function as recombination center, therefore the photocatalytic activity of the CdS will be declined a lot such as doped CdS samples with 3% and 5% Ag^+ in the reactants. This mechanism can be clearly implied in the following reaction equations

$$e^-_{CB} + Ag_n \rightarrow Ag_n^- \quad (1)$$

$$Ag_n^- + O_2 \rightarrow O_2^{\cdot-} + Ag_n \quad (2)$$

$$Ag_n^- + h^+ \rightarrow Ag_n \quad (3)$$

For small n the reaction equations are (1) and (2) .When the n is sufficiently large, reaction (3) will compete with (2), and the Ag_n will become the recombination center, thus the photocatalytic activity will be declined. In this photocatalytic degradation experiment, the photocatalytic degradation activity difference between the pure CdS and Ag-doped CdS with 1% Ag^+ in the reactants is small. This may be owing to the amounts of Ag which doped in CdS with 1%

Table 2
Photodegradation of Rhodamine B using CdS with different Ag-doped ratios as photocatalysts: (a) pure CdS; (b) 1% Ag^+ (0.025 mmol $AgNO_3$); (c) 3% Ag^+ (0.075 mmol $AgNO_3$); and (d) 5% Ag^+ (0.125 mmol $AgNO_3$).

Sample	First-order kinetics equation ($C = C_0e^{-Kt}$)	Coefficient constant (R^2)	Half-life (min)
a	$C_t = 3.67607e^{-0.03067t}$	0.99549	23
b	$C_t = 3.63252e^{-0.036t}$	0.98549	19
c	$C_t = 3.74674e^{-0.0113t}$	0.98259	61
d	$C_t = 3.64266e^{-0.0102t}$	0.99935	68